Evaluating the Performance of Extended EWMA Control Chart for Detecting Changes in Seasonal AR with Trend Models: An Application to Commodity Price Series

Yupaporn Areepong, Kotchaporn Karoon

***Abstract*—The Average Run Length (*ARL*) is a key indicator for evaluating how well control charts identify shifts. The purpose of this study is to derive explicit formula *ARL* and compare to *ARL* values obtained from numerical integral equation (NIE) techniques, such as the Midpoint, Simpson's, and Trapezoidal rules, in order to determine explicit formulas for the Extended Exponentially Weighted Moving Average (Extended EWMA) control chart and assess its performance. The suggested method is created using an exponential white noise seasonal autoregressive ($SAR(P)_L$) model with trend component. Banach's Fixed Point Theorem was used to ensure the uniqueness of the explicit *ARL* solution after the solution was derived using the Fredholm integral equation. Almost instantaneous results were obtained in practice, and the resulting expression greatly surpassed the *ARL* values produced by NIE techniques in terms of processing speed. The suggested extended EWMA control chart's greater efficiency is demonstrated using data on commodity prices series, especially those of gold and silver, which show significant volatility as a result of market dynamics. They make excellent candidates for statistical monitoring because of their susceptibility to variations, where early identification of structural changes is essential for financial risk management and well-informed decision-making.**

***Index Terms*— average run length, explicit formula, extended EWMA control chart, numerical integral equation**

I. Introduction

ONE significant and effective method for tracking and improving several processes across numerous industries is statistical process control, or SPC. Control charts are a core tool in Statistical Process Control (SPC), commonly applied to monitor ongoing processes and detect early signs of variation or unexpected behavior. This enables timely identification of anomalies and emerging trends during real-time operations.

The concept of control charts was first introduced by Shewhart [1], whose chart was designed to identify major deviations in process parameters. Since then, more sensitive tools such as the Cumulative Sum (CUSUM) chart [2] and the Exponentially Weighted Moving Average (EWMA) chart [3] have been developed to effectively capture small to moderate shifts in the process mean, offering improved detection capabilities over traditional charts. Furthermore, for processes where the data are both autocorrelated and from an independently normal distribution, Khan et al. [4] improved upon the modified exponentially weighted moving average (Modified EWMA) control chart, which had previously been developed by Patel and Divecha [5]. In 2010, Mahmoud and Woodall [6] modified the double exponentially weighted moving average (Double EWMA) control chart, which was originally introduced by Shamma and Shamma [7], and demonstrated that it provides greater sensitivity in detecting subtle changes in process parameters. Afterwards, the extended exponentially weighted moving average (Extended EWMA) control chart, proposed by Naveed et al. [8] in 2018, is an enhanced version of the traditional EWMA chart designed to more effectively detect subtle changes in process parameters. In real-world applications, control charts have been utilized across a wide range of fields, including healthcare, energy, finance, and environmental monitoring, demonstrating their versatility beyond traditional industrial contexts. In particular, Waqas et al. [9] conducted a systematic review and bibliometric analysis highlighting the extensive application of control charts, especially the EWMA chart, in hospital quality monitoring systems. Raza et al. [10] showed that the DEWMA-based control chart outperformed traditional control charts in terms of detection sensitivity and accuracy when applied to monitor censored recovery durations in cancer patients. In a review of control chart applications in finance, Bisiotis et al. [11] emphasized their effectiveness in tracking time series data related to stock prices, trading strategies, and risk management metrics.

The two-component average run length (*ARL*) is frequently used to assess a control chart's performance. The estimated number of samples from an in-control process before a false alert arises is represented by ARL_0, which should be as large as feasible to reduce false alarms. On the other hand, ARL_1, which represents the expected number of observations from an out-of-control process before a true alarm is triggered, should be minimized to enable timely detection of actual process shifts.

Manuscript received June 1, 2025; revised July 28, 2025.

This work was supported by Naresuan University (Thailand) and the National Science, Research and Innovation Fund (NSRF, Thailand) under Grant No. R2568B039.

Y. Areepong is a Professor in the Department of Applied Statistics, King Mongkut's University of Technology North Bangkok, Bangkok, 10800, Thailand (e-mail: yupaporn.a@sci.kmutnb.ac.th).

K. Karoon is an Assistant Professor in Department of Mathematics, Faculty of Science, Naresuan University, Phitsanulok, 65000, Thailand (corresponding author to provide e-mail: kotchapornk@nu.ac.th).

Various techniques have been employed to estimate the ARL, including Monte Carlo simulation [12], Markov chain analysis [13], and the numerical integral equation (NIE) method using quadrature rules such as the midpoint, trapezoidal, and Simpson's rules [14 -16].

Subsequently, several researchers proposed explicit formulas for computing the *ARL* and used these methods to verify the accuracy of their results.

Autocorrelation refers to the statistical dependence between successive observations in a time series. Control charts are widely used statistical tools for detecting shifts in process behavior; however, their effectiveness may be compromised when autocorrelation is present. Among these, SARIMA models, which are capable of capturing both seasonal patterns and linear or quadratic trends, are particularly effective in modeling the complex behaviors typically found in real-world time series. Such data often exhibit both periodic fluctuations and long-term trends.

Numerous empirical investigations have confirmed the effectiveness of this approach. For example, Chen [17] applied the SARIMA model to the automotive sector by analyzing and forecasting new and used car sales in the United States. The results showed that SARIMA successfully captured both long-term trends and seasonal fluctuations, leading to accurate sales forecasts. Similarly, Rono, Muriithi, and Mwangi [18] employed the SARIMA model to forecast outpatient visits, with the goal of enhancing healthcare planning through accurate short-term predictions.

Forecast error, defined as the difference between actual and predicted values, is a key indicator of model accuracy. Lower error values typically indicate better model performance. Although forecast errors are commonly assumed to be uncorrelated and normally distributed (i.e., white noise), real-world time series data, especially those with autocorrelation or seasonality, may generate errors that follow an exponential white noise pattern. This deviation from standard assumptions necessitates the use of more advanced modeling techniques.

Many academics have also developed precise formulas for calculating the Average Run Length (*ARL*) of various types of control charts. To illustrate, Suriyakat and Petcharat [19] provided an explicit formula for the *ARL* of an EWMA chart incorporating exogenous variables and a stationary moving average process. Zhang et al. [20] proposed explicit formulas for the performance evaluation of the CUSUM chart under an $SMA(Q)_S$ process with exponential white noise. An explicit formula for the *ARL* of a double moving average (DMA) control chart is proposed by Raweesawat and Sukparungsee [21] to track the process mean of a ZIPINAR(1) model. Later, Evaluating the *ARL* for a Shift in the Mean of a Long-Memory ARFIMA(1, d, 1)$(1, D, 1)_S$ model with exponential white noise operating on CUSUM chart was represented by Peerajit [22]. The *ARL* of the EWMA control chart, under the $SARX(P, r)_L$ model, can be accurately determined using the method introduced by Phanyaem [23]. Moreover, the extended EWMA control chart for AR(p) with Exogenous Variables was proposed by Muangngam et al. [24] for performance evaluation. Recently, Sunthornwat et al. [25] proposed explicit formulas for the *ARL* of the double DEWMA control chart applied to an $SMA(Q)_S$ process with exponential white noise. Karoon and Areepong [26] evaluated *ARL* performance of new extended EWMA control chart by comparing it with the standard and previously extended EWMA charts. They also provided an explicit *ARL* solution for the new chart under AR model, using a Thai economic dataset for empirical comparison.

Numerous researchers have formulated explicit expressions for *ARL* based on the $SAR(P)_L$ model, incorporating trend components into various types of control charts. These enhanced models have demonstrated improved effectiveness in detecting process shifts. Beginning in 2022, Petcharat [27] developed specific formulations for the *ARL* of CUSUM control charts based on the $SAR(P)_L$ model with a trend component, utilizing silver price data (USD/oz) for validation. Subsequently, in 2023, Areepong and Karoon [28] utilized observations from a seasonal autoregressive model to enhance usability by deriving exact formulas for the *ARL* applied to a double EWMA control chart. Air pollution, which is one of Thailand's critical environmental issues, was selected as the application context for the study. In the following year, 2024, Areepong and Karoon [29] extended their previous work by deriving explicit ARL formulas based on a seasonal autoregressive model with an added trend component. This enhanced approach was further applied to a GDP dataset in Thailand. In 2025, Sukparungsee and Areepong [30] proposed an explicit *ARL* formula using an integral equation approach for the double modified EWMA chart under the $SAR(P)_L$ process.

To the best of our knowledge, no prior studies have presented explicit *ARL* formulas for an extended EWMA control chart based on the trend $SAR(P)_L$ model with exponential white noise. This study addresses that research gap by deriving an exact *ARL* expression for the extended EWMA chart within the trend $SAR(P)_L$ framework. The proposed approach builds upon and extends the earlier work of Karoon et al. [29], who previously examined control chart performance under the $SAR(P)_L$ model without a trend component. The performance of the explicit *ARL* formulas is compared between the conventional and extended EWMA control charts using both simulated and real-world datasets. To demonstrate the effectiveness of the proposed method, gold and silver price series, which are well known for their high volatility, are used. Their significant fluctuations make them appropriate for statistical monitoring and the early detection of structural changes.

II. Material and Methods

A. Structures of Control Charts

To begin with, the concept of the traditional EWMA control chart was introduced by Roberts [3], who demonstrated its effectiveness in identifying minor shifts in process behavior. The EWMA statistic in Eq. (1) is computed using the following formula:

$$Ew_t = (1-\lambda)Ew_{t-1} + \lambda Y_t, t = 1, 2, \ldots \quad (1)$$

where Y_t is a sequence of trend $SAR(P)_L$ model with operating based on exponential white noise, λ represents the exponential smoothing parameter with interval as $(0 < \lambda_1 \leq 1)$. The EWMA control chart's control boundaries are as

$$\mu_0 \pm K\sigma\sqrt{\frac{\lambda}{2-\lambda}},$$

where K denotes the width of the control limits of EWMA. μ_0 is the mean whereas σ is the mean and the standard deviation of the process, which are obtained from the variance (σ^2) of the EWMA statistic as $\sigma^2\left[\frac{\lambda}{2-\lambda}\right]$. Mathematically, the stopping time is formulated as: $\tau_{Ew} = \inf\{t \geq 0 : Ew_t < r', Ew_t > s'\}$ and then r' and s' are showed as the lower (LCL) and upper (UCL) control limit of EWMA control chart.

Building upon Roberts' [3] introduction of the EWMA control chart for monitoring processes over time, Naveed [8] developed the extended EWMA control chart. This enhanced version demonstrates strong performance in detecting subtle deviations from the process behavior. Using the recursive equation in Eq. (2) below, the extended EWMA control chart can be expressed.

$$Ex_t = \lambda_1 Y_t - \lambda_2 Y_{t-1} + (1-\lambda_1+\lambda_2)Ex_{t-1}, t = 1,2,... \quad (2)$$

where λ_1 and λ_2 are exponential smoothing parameters with interval as $(0 < \lambda_1 \leq 1)$ and $(0 < \lambda_2 < \lambda_1)$, respectively. Moreover, A represents $1-\lambda_1+\lambda_2$. The upper and lower control limits appeared as follows on the Extended EWMA chart:

$$\mu_0 \pm \hat{K}\sigma\sqrt{\frac{\lambda_1^2+\lambda_2^2-2\mathrm{A}\lambda_1\lambda_2}{2(\lambda_1-\lambda_2)-(\lambda_1-\lambda_2)^2}},$$

where μ_0 and σ represent the mean, the process standard deviation as mentioned previously, σ rewritten from the variance (σ^2) of extended EWMA statistic as follows below $\sigma^2\left[\frac{\lambda_1^2+\lambda_2^2-2\mathrm{A}\lambda_1\lambda_2}{2(\lambda_1-\lambda_2)-(\lambda_1-\lambda_2)^2}\right]$, and then $\hat{K}$ denotes the width of the control limits of Extended EWMA. The stopping time can be expressed by the following equation: $\tau_{Ex} = \inf\{t \geq 0 : Ex_t < r, Ex_t > s\}$ where r and s are illustrated as the lower (LCL) and upper (UCL) control limit of Extended EWMA control chart. More importantly, if λ_2 instead of 0 in Eq. (2), the Extended EWMA statistic transforms into the EWMA statistic.

B. Methodology of Derivation Explicit ARL Formula under Trend SAR(P)$_L$ Model

This study uses the general trend seasonal autoregressive model, commonly referred to as the trend SAR(P)$_L$ model, a statistical technique for examining time-series data, to construct exact *ARL* formulas. This model, which incorporates seasonal patterns and trends, is widely utilized in disciplines like engineering and economics. The following Eq. (3) contains its formulation.

$$Y_t = \eta + \omega t + \phi_1 Y_{t-1L} + \phi_2 Y_{t-2L} + ... + \phi_P Y_{t-PL} + \xi_t \quad (3)$$

where η is the constant of trend SAR(P)$_L$ model, ω represents the constant term or trend component, which is treated as an exogenous variable to capture the underlying trend or time of the data. $\phi_t, t = 1,2,...,P$ denote the coefficients of time series model with $\phi_1, \phi_2, ..., \phi_P \in (-1,1)$. In this context, L denotes the seasonal length, where L = 4 corresponds to quarterly data and L = 12 corresponds to monthly data. Also, ξ_t denotes the error term, assumed to be a continuous i.i.d. random variable derived from exponential white noise.; $\xi_t \sim Exp(\alpha)$. The probability density function of ξ_t can be showed as

$$f(y,\alpha) = 1/\alpha e^{-y/\alpha}; \alpha > 0.$$

Guided by the ARL characteristics explored in this study, several change-point models are analyzed as follows.

$$\xi_t \sim \begin{cases} Exp(\alpha_0), & t = 1,2,...,\beta-1 \\ Exp(\alpha_1), & t = \beta, \beta+1, ... \end{cases} \quad (4)$$

where α_0 and α_1 are known parameters, which α_0 represents the mean of exponential distribution , and $\alpha_1 > \alpha_0$. By exploring the change point in Eq. (4), the *ARL* defined with $E_\beta(.)$ can be explained as follows.

$$ARL = \begin{cases} ARL_0 = E_\infty(\tau), \beta = \infty & (no \quad change) \\ ARL_1 = E_1(\tau), \beta = 1 & (change) \end{cases},$$

where $E_\beta(.)$ is the mean under exponential distribution $f(y,\alpha)$ for a given change-point time. $\beta = \infty$ shows in-control which stands for ARL_0, whereas $\beta = 1$ Represents the first occurrence of a shift from α_0 to α_1 in the process, which is known as out-of-control *ARL* which stands for ARL_1.

In this Study, let ξ_t denote the Extended EWMA statistic, with a change-point occurring at time $t = 1$. Then, using the trend SAR(P)$_L$ model, the statistic defined in Eq. (2) can be reformulated as follows:

$$Ex_1 = \lambda_1(\theta + \xi_1) - \lambda_2 Y_{1-1L} + \mathrm{A}Ex_0$$

where θ represents $\eta + \omega + \phi_1 Y_{1-1L} + \phi_2 Y_{1-2L} + ... + \phi_P Y_{1-PL}$.

The extended EWMA control chart, under the in-control state, functions as a two-sided control chart when both upper and lower thresholds are considered. So that, $r < Ex_t < s$. It can be rewritten as follows:

$$r < \lambda_1(\theta + \xi_1) - \lambda_2 Y_{1-1L} + \mathrm{A}Ex_0 < s$$
$$r < \lambda_1\theta + \lambda_1\xi_1 - \lambda_2 Y_{1-1L} + \mathrm{A}Ex_0 < s$$
$$\frac{r - \mathrm{A}Ex_0 + \lambda_2 Y_{1-1L}}{\lambda_1} - \theta < \xi_1 < \frac{s - \mathrm{A}Ex_0 + \lambda_2 Y_{1-1L}}{\lambda_1} - \theta .$$

Assume the initial values are given by $Ex_0 = \varpi$. The interval (ξ_t) can be transformed into the form:

$$\frac{r - \mathrm{A}\varpi + \lambda_2 Y_{1-1L}}{\lambda_1} - \theta < \xi_1 < \frac{s - \mathrm{A}\varpi + \lambda_2 Y_{1-1L}}{\lambda_1} - \theta .$$

Let $\vartheta(\varpi)$ be the explicit *ARL* formula running on extended EWMA control chart under trend SAR(P)$_L$ model. As shown below, a modification based on the Fredholm integral equation of the second kind [32] was used to get the explicit *ARL* formula in this investigation.

$$\vartheta(\varpi) = 1 + \int_{q}^{q'} \vartheta\left(\lambda_1(\theta + \xi_1) - \lambda_2 Y_{1-1L} + \mathrm{A}\varpi\right) f(\xi_1) d\xi_1$$

where q and q' represent $\frac{r - \mathrm{A}\varpi + \lambda_2 Y_{1-1L}}{\lambda_1} - \theta$ and $\frac{s - \mathrm{A}\varpi + \lambda_2 Y_{1-1L}}{\lambda_1} - \theta$, respectively.

Let ψ denotes $\lambda_1(\theta + \xi_1) - \lambda_2 Y_{1-1L} + \mathrm{A}\varpi$, and then $\frac{d\psi}{d\xi_1} = \lambda_1$ whereas $d\xi_1 = \frac{1}{\lambda_1} = d\psi$.

The integral variable of $\vartheta(\varpi)$ was changed; This expression can be rearranged as Eq. (5), presented below.

$$\vartheta(\varpi) = 1 + \frac{1}{\lambda_1}\int_{r}^{s} \vartheta(\psi) f\left(\frac{\psi - \mathrm{A}\varpi + \lambda_2 Y_{1-1L}}{\lambda_1} - \theta\right) d\psi. \quad (5)$$

When consider that $\varepsilon_1 \sim Exp(\alpha)$, the second-kind Fredholm integral equation can be used to get the explicit *ARL* formula, which is as follows:

$$\vartheta(\varpi) = 1 + \frac{\mathrm{H}(\varpi)}{\lambda_1\alpha} \cdot \Lambda \quad (6)$$

where $\mathrm{H}(\varpi) = \exp\left(\frac{\mathrm{A}\varpi - \lambda_2 Y_{1-1L}}{\lambda_1\alpha} + \frac{\theta}{\alpha}\right)$,

$\Lambda = \int_{r}^{s} \vartheta(\psi)\Lambda_0(\psi) d\psi$, and $\Lambda_0(\psi) = \exp\left(-\frac{\psi}{\lambda_1\alpha}\right)$.

According to Eq. (6), the following relationship holds:

$$\Lambda = \int_{r}^{s} \Lambda_0(\psi)\left(1 + \frac{\mathrm{H}(\varpi)}{\lambda_1\alpha}\right) d\psi$$
$$= -\frac{\alpha\lambda_1\left[\Lambda_0(s) - \Lambda_0(r)\right]}{1 + \frac{1}{\Omega}\exp\left(\frac{\lambda_2 Y_{1-1L}}{\lambda_1\alpha} - \frac{\theta}{\alpha}\right)\cdot\left[\Lambda_0(\Omega\cdot s) - \Lambda_0(\Omega\cdot r)\right]}, \quad (7)$$

where Ω denotes $\lambda_1 - \lambda_2$ as seen in Eq. (7).

In the next step, Eq. (5) is proven using Banach's fixed-point theorem [33] to verify the existence and uniqueness of the *ARL* solution for the extended EWMA control chart applied to the trend SAR(P)$_L$ process. The procedure is outlined as follows and further detailed in the Appendix.

Once the uniqueness of the *ARL* has been confirmed, new variables can be added to Eq. (7) to change it. The exact *ARL* for the extended EWMA control chart under the trend SAR(P)$_L$ model can therefore be represented by rearranging the equation, as shown in Eq. (8) below.

$$\vartheta(\varpi) = 1 - \frac{\Omega\cdot\Lambda_0(\mathrm{A}\varpi)\cdot\left[\Lambda_0(s) - \Lambda_0(r)\right]}{\Omega\cdot\exp\left(\frac{\lambda_2 Y_{1-1L}}{\lambda_1\alpha} - \frac{\theta}{\alpha}\right) + \left[\Lambda_0(\Omega\cdot s) - \Lambda_0(\Omega\cdot r)\right]}. \quad (8)$$

In addition to Eq. (8), assigning $\alpha = \alpha_0$ corresponds to the in-control condition, while $\alpha = \alpha_1 = \alpha_0(1+\delta)$ may be interpreted as representing the out-of-control situation.

C. Methodology of ARL by NIE Techniques under Trend SAR(P)$_L$ Model

At this point, the Numerical Integral Equation (NIE) method is employed to analyze the Trend SAR(P)$_L$ model. According to Equation (5), the Average Run Length (*ARL*) of the extended EWMA control chart is numerically approximated by solving a system of m linear equations. The resulting *ARL* estimates, denoted by $\vartheta'(\varpi)$ correspond to the use of classical quadrature techniques, such as Midpoint ($\vartheta'_M(\varpi)$), Simpson's ($\vartheta'_S(\varpi)$), and Trapezoidal ($\vartheta'_T(\varpi)$) rules, respectively. These quadrature techniques are applied over the integration domain, as described in [14]. Moreover, these methods are defined by a set of nodes $\{c_j, j = 0,1,2,...,m\}$, which are generated by partitioning the integration interval $[r,s]$ into m subintervals, together with a corresponding set of weights $\{w_j, j = 0,1,2,...,m\}$ Typically, the integral is approximated using the following expression:

$$\int_{r}^{s} W(c) f(c) dc \approx \sum_{j=1}^{m} w_j f(c_j) .$$

The quadrature method leads to the result shown below.

$$\mathcal{G}'(c_i) = 1 + \frac{1}{\lambda_1}\sum_{j=1}^{m} w_j \cdot \mathcal{G}'(c_j) \cdot f\left(\frac{c_j - \mathrm{A}c_i + \lambda_2 Y_{1-1L}}{\lambda_1} - \theta\right), i = 1, 2, ..., m.$$

The resulting system consists of m linear equations and can be represented as a vector $Q_{m\times 1} = (I_m - R_{m\times m})^{-1} 1_{m\times 1}$

where $Q_{m\times 1} = [\mathcal{G}'(c_1) \quad \mathcal{G}'(c_2) \quad ... \quad \mathcal{G}'(c_m)]^T$.

Let $R_{m\times m}$ be a matrix and define the m to m^{th} as elements of matrix R as follows,

$$[R_{ij}] \approx \frac{1}{\lambda_1} w_j f\left(\frac{c_j - \mathrm{A}c_i + \lambda_2 Y_{1-1L}}{\lambda_1} - \theta\right).$$

In conclusion, ϖ is used instead of c the numerical formulation for approximating $\mathcal{G}'(\varpi)$ is given by

$$\mathcal{G}'(\varpi) = 1 + \frac{1}{\lambda_1}\sum_{j=1}^{m} w_j \mathcal{G}'(c_j) \cdot f\left(\frac{c_j - \mathrm{A}\varpi + \lambda_2 Y_{1-1L}}{\lambda_1} - \theta\right). \quad (9)$$

The details of various composite quadrature rules, including the locations of nodes and their corresponding weights, are presented based on equal subinterval widths $h = (s - r)/m$, and are summarized in Table I. below. Also, the expression for M_j, defined as: $\frac{c_j - \mathrm{A}\varpi + \lambda_2 Y_{1-1L}}{\lambda_1} - \theta$ listed in the same table.

TABLE I
THE COMPOSITE QUADRATURE RULES

Rules	Formulas
Midpoint	$\mathcal{G}'_M(\varpi) = 1 + \frac{1}{\lambda_1}\sum_{j=1}^{m} w_j \mathcal{G}'(c_j) \cdot f\left(M_j\right)$
Node (c_j)	$r + (j - 0.5)h$
Weight (w_j)	h
Simpson's	$\mathcal{G}'_S(\varpi) = 1 + \frac{1}{\lambda_1}\sum_{j=0}^{2n} w_j \mathcal{G}'(c_j) \cdot f\left(M_j\right)$, where $m = 2n$
Node (c_j)	$r + jh$
Weight (w_j)	$\frac{h}{3}; j = 0, 2n, \frac{4h}{3}; j = 1, ..., 2n-1, \frac{2h}{3}; j = 2, ..., 2n-2$
Trapezoidal	$\mathcal{G}'_T(\varpi) = 1 + \frac{1}{\lambda_1}\sum_{j=0}^{m} w_j \mathcal{G}'(c_j) \cdot f\left(M_j\right)$,
Node (c_j)	$r + jh$
Weight (w_j)	$\frac{h}{2}; j = 0, m, h; j = 1, ..., m-1$

III. Experimental Results and Performance Evaluation of Control Chart

This section compares the explicit *ARL* formula from the Fredholm integral equation with the NIE-based *ARL* using composite quadrature rules including Midpoint, Simpson's, and Trapezoidal rules under the extended EWMA control chart with 1,000 nodes. The trend SAR(P)$_L$ model is used for data analysis. Let $\mathcal{G}(\varpi)$ and $\mathcal{G}'(\varpi)$ represent the *ARL* values derived from the NIE technique and the explicit formula via Eq. (8) and (9), respectively. The absolute percentage relative error or APRE(%) between them is measured using Eq. (10).

$$\mathrm{APRE}(\%) = \left|\frac{\mathcal{G}(\varpi) - \mathcal{G}'(\varpi)}{\mathcal{G}(\varpi)}\right| \times 100\% \quad (10)$$

The *ARL* estimation using the NIE method was performed with 1,000 division points. The details of the *ARL* evaluation are presented in Table II below.

TABLE II
THE PROCEDURING OF ARL EVALUATION

Input:	Provide the following input values to run the program:
	Set parameters of trend SAR(P)$_L$ model: $\eta, \omega,$ and ϕ_t in Eq. (3).
	Set parameters of control charts: $\lambda_1 = 0.05, 0.10, 0.15$, $\lambda_2 = 0.015, 0.03, 0.045$ for extended EWMA chart, $\lambda_2 = 0$ for EWMA chart.
	Set the lower control limit (LCL) equal to r.
	Set $ARL_0 = 370$ for simulated data, whereas real-world data were set to 370 and 500.
	Set $\alpha = \alpha_0$ for in-control, set $\alpha_0 = 1$ when using simulated data, whereas set α_0 equal to the exponential mean $(\xi_t \sim Exp(\alpha))$ when using a real-world data.
	Set $\alpha = \alpha_1 = \alpha_0(1 + \delta)$ for out-of-control, and δ equal $0.0005, 0.001, 0.002, 0.005, 0.01, 0.03, 0.1, 0.5$.
Output:	The output generated by the program is as follows:
	The Upper Control Limit (UCL) of the control chart under various parameter settings is defined based on a specified in-control *ARL*.
	The *ARL* under the out-of-control condition is calculated by setting the UCL according to the specified criteria above.

These results, summarized in Table III, are based on the trend SAR(1)$_4$, trend SAR(2)$_4$, and trend SAR(3)$_4$ models. All computations were performed on a Windows 10 (64-bit) platform with an Intel Core i5-8250U processor (1.60–1.80 GHz) and 4 GB of RAM. In all scenarios, the absolute percentage relative error is minimal, approaching 0%, which indicates that both approaches provide comparable accuracy. In particular, Simpson's method yields errors ranging from 10^{-10} to less than 10^{-13}, demonstrating its high precision. However, the explicit formula yields results almost instantaneously across all cases. In contrast, *ARL* values generated using the NIE method with the three quadrature rules exhibit varied response times. Under the Midpoint and Trapezoidal rules, the system responds within 5 to 6 seconds, while with Simpson's rule, the response time ranges from 21 to 23 seconds. All computations were performed using the extended EWMA control chart with parameters set at UCL = r = 0. This suggests that the difference in computation time between the explicit formula and the NIE technique using the three quadrature rules is relatively small. While the explicit solution remains unaffected by CPU specifications, the computation time required by the NIE method is influenced by the processor's performance.

Next, the *ARL* based on the explicit formula for different extended EWMA settings was then compared to the traditional EWMA chart. The simulated data is typically generated $ARL_0 = 370$ to represent the in-control condition. The initial parameters used for the study are specified in Table II referenced above. Besides, to evaluate the efficiency of control charts, the Average Extra Quadratic Loss (AEQL) is employed as a supporting metric. The method for calculating AEQL is shown in Eq. (11) [26].

$$\mathrm{AEQL} = \frac{1}{\Delta}\sum_{\delta_i=\delta_{\min}}^{\delta_{\max}}\left(\delta_i^2 \times \left(1 - \frac{\Omega\cdot\Lambda_0(\mathrm{A}\varpi)\cdot G'}{G''+G'''}\right)\right), \tag{11}$$

where

G' denotes $\exp\left(-\frac{s}{\lambda_1(\alpha_0+\alpha_0\delta_i)}\right) - \exp\left(-\frac{r}{\lambda_1(\alpha_0+\alpha_0\delta_i)}\right)$,

G'' denotes $\Omega\cdot\exp\left(\frac{\lambda_2 Y_{1-1L}}{\lambda_1(\alpha_0+\alpha_0\delta_i)} - \frac{\theta}{\alpha_0+\alpha_0\delta_i}\right)$, and

G''' denotes $\exp\left(-\frac{\Omega\cdot s}{\lambda_1(\alpha_0+\alpha_0\delta_i)}\right) - \exp\left(-\frac{\Omega\cdot r}{\lambda_1(\alpha_0+\alpha_0\delta_i)}\right)$.

δ_i indicates the process shift magnitude monitored by the control chart

Δ represents the total number of shift values ranging from point $\delta_{\min}$ to point $\delta_{\max}$. In this study, Δ was defined as 8 incremental steps, uniformly distributed from 0.0005 to 0.5.

Among the evaluated charts, this control chart produces the lowest AEQL, suggesting its higher capability in detecting process shifts. Also, the Performance Comparison Index (PCI) is calculated based on the AEQL values of each control chart. Specifically, PCI is defined as the ratio of a control chart's AEQL to the minimum AEQL among all charts under consideration. This provides a standardized basis for comparing the performance of different control charts. PCI can be mathematically expressed in Eq. (12) as:

$$\mathrm{PCI} = \mathrm{AEQL}/\mathrm{AEQL}_{\mathrm{Lowest}} \tag{12}$$

PCI value of 1 typically signifies optimal control chart performance, characterized by rapid detection of process shifts and a low rate of false alarms.

Table IV presents the results corresponding to the trend SAR(1)$_4$ and trend SAR(2)$_4$ models, and the lower and upper control limits are analyzed within the intervals [0, s] for the extended EWMA chart and [0, s'] for the traditional EWMA chart, respectively. This study determined the coefficient λ_1 to be $\lambda_1 = 0.05, 0.10,$ and 0.15, whereas λ_2 was determined as $\lambda_2 = 0.015, 0.03,$ and 0.045. The findings revealed that the explicit *ARL* achieved by the extended EWMA control chart outperforms that of the traditional EWMA chart under various settings of the smoothing parameters. Notably, the extended EWMA chart with a fixed $\lambda_1 = 0.05$ exhibited superior performance. When comparing each case separately based on the value of λ_1, the extended EWMA chart with a fixed $\lambda_2 = 0.045$ exhibited the lowest ARL_1 value compared to both the extended EWMA charts with other fixed $\lambda_2 = 0.03$ and $\lambda_2 = 0.015$, as well as the traditional EWMA chart with a fixed $\lambda_2 = 0$. Moreover, a decrease in λ_2, particularly when it approaches zero, is associated with a reduction in ARL_1, indicating enhanced sensitivity in detecting shifts in the process mean. The results remained equivalent in all scenarios. Furthermore, the extended EWMA control chart with $\lambda_2 = 0.045$ achieved the lowest ARL_1 across all levels of shift. Its PCI value was equal to 1, confirming the superior performance of the extended EWMA chart in all cases under both the SAR(1)$_4$ and SAR(2)$_4$ models.

Table V presents the results corresponding to the trend SAR(3)$_4$ model, and the lower and upper control limits are analyzed within the intervals [r, s] for the extended EWMA chart and [r, s'] for the traditional EWMA chart, respectively. The findings revealed that the explicit ARL obtained from the extended EWMA control chart with fixed $\lambda_1 = 0.05$ and $\lambda_2 = 0.045$ values resulted in the lowest ARL_1 across all levels of the lower control limit (LCL), or r from 0 to 0.1. values, when compared to the traditional EWMA chart with fixed $\lambda_1 = 0.05$ and $\lambda_2 = 0$. The corresponding AEQL and PCI values further support the superior performance of the extended EWMA control chart.

TABLE III
COMPARING *ARL* VALUES OF EXPLICIT FORMULAS AGAINST THE NIE TECHNIQUES USING THREE QUADRATURE RULES ON EXTENDED EWMA CONTROL CHART BASED ON THE TREND SAR(P)$_L$ MODELS GIVEN $r = 0, \eta = 0.5, \lambda_1 = 0.05, \lambda_2 = 0.03$

Models	Shift sizes (δ)	Explicit Formula (CPU Time)	NIE techniques (CPU Time, APRE(%))		
			Midpoint	Simpson's	Trapezoidal
Trend SAR(1)$_4$ $\omega = 0.15$, $\phi_1 = 0.1$, $s = 0.0123306$	0	370.09538109175 (<0.1)	370.09538000105 (5.359, 2.947E-07)	370.09538109179 (21.828, 9.722E-12)	370.09538327327 (5.438, 5.894E-07)
	0.0005	247.18794895004 (<0.1)	247.18794825758 (5.640, 2.801E-07)	247.18794894989 (22.140, 5.947E-11)	247.18795033451 (5.341, 5.601E-07)
	0.001	185.67418795099 (<0.1)	185.67418744526 (5.406, 2.724E-07)	185.67418795113 (21.844, 7.972E-11)	185.67418896287 (5.281, 5.450E-07)
	0.002	124.12037309129 (<0.1)	124.12037276322 (5.547, 2.643E-07)	124.12037309119 (21.734, 8.298E-11)	124.12037374713 (5.375, 5.284E-07)
	0.005	62.526592053656 (<0.1)	62.526591895028 (5.562, 2.537E-07)	62.526592053667 (22.235, 1.791E-11)	62.526592370943 (5.453, 5.074E-07)
	0.01	34.516446386304 (<0.1)	34.516446301791 (5.531, 2.449E-07)	34.516446386305 (22.422, 8.646E-13)	34.516446555333 (5.437, 4.897E-07)
	0.03	12.826801839586 (<0.1)	12.826801811186 (5.422, 2.214E-07)	12.826801839585 (22.063, 3.905E-12)	12.826801896384 (5.422, 4.428E-07)
	0.1	4.5624952480772 (<0.1)	4.5624952406044 (5.359, 1.638E-07)	4.5624952480771 (22.125, 1.752E-12)	4.562495263022 (5.453, 3.276E-07)
	0.5	1.6617302103017 (<0.1)	1.6617302095562 (5.484, 4.486E-08)	1.6617302103017 (21.922, <1.000E-13)	1.661730211793 (5.406, 8.972E-08)
Trend SAR(2)$_4$ $\omega = -0.15$, $\phi_1 = 0.1$, $\phi_2 = -0.3$, $s = 0.02251843$	0	370.025432811 (<0.1)	370.02542912226 (5.391, 9.969E-07)	370.02543281023 (21.953, 2.021E-10)	370.02544018616 (5.437, 1.993E-06)
	0.0005	262.642475051 (<0.1)	262.64247255658 (5.514, 9.497E-07)	262.64247505142 (21.734, 1.736E-10)	262.64248004111 (5.391, 1.900E-06)
	0.001	203.669229490 (<0.1)	203.66922760956 (5.546, 9.234E-07)	203.66922949028 (22.047, 2.946E-11)	203.66923325170 (5.406, 1.847E-06)
	0.002	140.697292251 (<0.1)	140.69729099369 (5.578, 8.935E-07)	140.69729225082 (22.015, 9.939E-12)	140.69729476508 (5.719, 1.787E-06)
	0.005	73.305662416 (<0.1)	73.305661789383 (5.609, 8.548E-07)	73.305662416011 (22.610, 5.211E-11)	73.305663669266 (5.906, 1.710E-06)

		41.084095633	41.084095294179	41.084095632838	41.084096310156
	0.01	(<0.1)	(5.500, 8.243E-07)	(22.203, 2.653E-11)	(5.547, 1.649E-06)
		15.411499219	15.411499103308	15.411499218926	15.411499450162
	0.03	(<0.1)	(5.469, 7.502E-07)	(21.953, 3.239E-12)	(5.516, 1.500E-06)
		5.451637637	5.4516376055193	5.4516376366793	5.4516376989992
	0.1	(<0.1)	(5.547, 5.716E-07)	(22.609, 3.747E-13)	(5.391, 1.143E-06)
		1.902762467	1.9027624634711	1.9027624668635	1.9027624736481
	0.5	(<0.1)	(5.500, 1.783E-07)	(22.297, 5.251E-13)	(5.516, 3.566E-07)
		370.05374463466	370.05374315876	370.05374463619	370.05374759106
	0	(<0.1)	(5.937, 3.988E-07)	(21.860, 4.132E-10)	(5.468, 7.989E-07)
		250.92364263122	250.92364167851	250.92364263131	250.92364453690
	0.0005	(<0.1)	(5.640, 3.797E-07)	(21.953, 3.228E-11)	(5.453, 7.595E-07)
		189.92569984580	189.92569914401	189.92569984547	189.92570124841
	0.001	(<0.1)	(5.531, 3.695E-07)	(22.454, 1.753E-10)	(5.500, 7.385E-07)
Trend SAR(3)$_4$		127.94162791314	127.94162745499	127.94162791306	127.94162882921
$\omega = 0.1$,	0.002	(<0.1)	(5.829, 3.581E-07)	(22.329, 6.019E-11)	(5.329, 7.160E-07)
$\phi_1 = 0.1$,		64.947406406113	64.947406182968	64.947406406084	64.947406852316
$\phi_2 = 0.2$,	0.005	(<0.1)	(5.547, 3.436E-07)	(21.813, 4.542E-11)	(5.484, 6.870E-07)
$\phi_3 = -0.3$,		35.973206677521	35.973206558256	35.973206677514	35.973206916030
$s = 0.01433248$	0.01	(<0.1)	(5.796, 3.315E-07)	(22.266, 1.807E-11)	(5.469, 6.630E-07)
		13.394110054708	13.394110014486	13.394110054709	13.394110135157
	0.03	(<0.1)	(5.407, 3.003E-07)	(21.829, 1.119E-11)	(5.453, 6.006E-07)
		4.7563141836773	4.7563141730306	4.7563141836771	4.7563142049701
	0.1	(<0.1)	(5.516, 2.238E-07)	(21.907, 3.156E-12)	(5.468, 4.477E-07)
		1.7133089357708	1.7133089346850	1.7133089357708	1.7133089379422
	0.5	(<0.1)	(5.406, 6.337E-08)	(21.922, <1.000E-13)	(5.500, 1.267E-07)

TABLE IV
COMPARING ARL_1 VALUES ON EXTENDED EWMA AND EWMA CHARTS FOR TREND SAR(P)$_L$ MODELS GIVEN $\alpha_0 = 1, r = 0, \omega = 0.35, \phi_1 = \phi_2 = 0.15,\ \eta = 0$ FOR TREND SAR(1)$_4$, $\eta = 0.1$ FOR TREND SAR(2)$_4$, AND ARL_0 = 370

λ_1	CC	λ_2	UCL	α_1								AEQL	PCI
				1.0005	1.001	1.002	1.005	1.01	1.03	1.1	1.5		
Trend SAR(1)$_4$													
0.05	Extended EWMA	0.015	0.02835617	269.33	211.82	148.57	78.69	44.44	16.75	5.92	2.03	0.074	1.251
		0.03	0.01796331	256.67	196.59	134.05	68.89	38.37	14.34	5.08	1.80	0.065	1.105
		0.045	0.01141779	245.12	183.37	122.09	61.26	33.76	12.53	4.46	1.64	0.059	1.000
	EWMA	0	0.05016143	284.39	231.04	168.14	92.87	53.55	20.48	7.20	2.37	0.087	1.472
0.10	Extended EWMA	0.015	0.0725189	277.97	222.67	159.43	86.41	49.34	18.74	6.59	2.20	0.080	1.159
		0.03	0.0572857	270.36	213.07	149.80	79.54	44.97	16.96	5.98	2.04	0.074	1.071
		0.045	0.04539605	263.46	204.65	141.63	73.93	41.47	15.56	5.50	1.91	0.069	1.000
	EWMA	0	0.0922101	286.69	234.08	171.37	95.33	55.16	21.14	7.41	2.42	0.088	1.276
0.15	Extended EWMA	0.015	0.1199609	282.50	228.55	165.52	90.89	52.24	19.92	6.99	2.30	0.084	1.124
		0.03	0.1019086	276.72	221.05	157.77	85.20	48.56	18.41	6.47	2.17	0.079	1.056
		0.045	0.08681223	271.37	214.34	151.05	80.41	45.52	17.18	6.05	2.05	0.075	1.000
	EWMA	0	0.14170883	289.05	237.24	174.76	97.94	56.88	21.84	7.64	2.46	0.090	1.208
Trend SAR(2)$_4$													
0.05	Extended EWMA	0.015	0.0220325	262.33	203.28	140.32	73.05	40.92	15.34	5.43	1.89	0.069	1.222
		0.03	0.01397751	250.30	189.21	127.29	64.53	35.72	13.30	4.72	1.70	0.061	1.095
		0.045	0.00889054	239.15	176.75	116.29	57.68	31.63	11.72	4.19	1.56	0.056	1.000
	EWMA	0	0.0348984	276.12	220.17	156.82	84.49	48.11	18.24	6.43	2.17	0.079	1.404
0.10	Extended EWMA	0.015	0.0560806	270.20	212.78	149.46	79.28	44.80	16.89	5.95	2.03	0.074	1.137
		0.03	0.0444095	263.11	204.22	141.22	73.65	41.30	15.49	5.47	1.90	0.069	1.062
		0.045	0.0352529	256.82	196.67	134.08	68.90	38.37	14.33	5.07	1.80	0.065	1.000
	EWMA	0	0.071057	277.81	222.38	159.09	86.14	49.16	18.66	6.56	2.19	0.080	1.231
0.15	Extended EWMA	0.015	0.0922742	273.88	217.47	154.17	82.61	46.91	17.74	6.24	2.10	0.076	1.103
		0.03	0.0786297	268.79	211.10	147.84	78.16	44.10	16.60	5.85	2.00	0.073	1.048
		0.045	0.067142	263.96	205.22	142.16	74.28	41.68	15.64	5.52	1.91	0.069	1.000
	EWMA	0	0.1085702	279.53	224.64	161.44	87.86	50.27	19.10	6.70	2.22	0.081	1.170

TABLE V
COMPARING ARL_1 VALUES ON EXTENDED EWMA ($\lambda_1 = 0.05, \lambda_2 = 0.045$) AND EWMA ($\lambda_1 = 0.05$) CHARTS FOR TREND SAR(3)$_4$ MODELS UNDER DIFFERENT LCL interval ($r = r'$) and , AND GIVEN $\alpha_0 = 1, \eta = \omega = 0.5, \phi_1 = \phi_3 = 0.2, \phi_2 = -0.25$ WHEN $ARL_0 = 370$

Trend SAR(3)$_4$											
LCL	CC	UCL	α_1								AEQL	PCI
			1.0005	1.001	1.002	1.005	1.01	1.03	1.1	1.5		
$r = 0$	Extended EWMA	0.01113566	244.55	182.71	121.50	60.89	33.54	12.45	4.43	1.63	0.059	1.000
	EWMA	0.0439062	283.66	229.96	166.93	91.94	52.93	20.22	7.11	2.35	0.087	1.472
$r = 0.0005$	Extended EWMA	0.0116365	243.82	181.85	120.72	60.40	33.25	12.34	4.40	1.62	0.058	1.000
	EWMA	0.0444294	282.94	229.08	166.06	91.30	52.52	20.06	7.06	2.34	0.085	1.463
$r = 0.005$	Extended EWMA	0.0161438	236.25	173.61	113.62	56.11	30.74	11.43	4.14	1.59	0.057	1.000
	EWMA	0.0491389	277.49	221.92	158.61	85.82	49.00	18.66	6.63	2.27	0.082	1.452
$r = 0.075$	Extended EWMA	0.08624068	113.46	67.37	37.50	16.57	9.00	3.76	1.89	1.23	0.042	1.000
	EWMA	0.1224766	167.39	108.45	63.97	29.20	15.78	6.24	2.77	1.55	0.053	1.276
$r = 0.1$	Extended EWMA	0.11127125	78.74	44.47	24.13	10.66	5.93	2.71	1.57	1.17	0.039	1.000
	EWMA	0.14871647	126.95	77.00	43.44	19.35	10.51	4.37	2.17	1.41	0.048	1.221

TABLE VI
TREND SAR(P)$_L$ MODEL ESTIMATION, MODEL FITS, AND WHITE NOISE TEST OF RESIDUALS FOR GOLD AND SILVER PRICES SERIES

Series	Models	Variables	Estimate	SE.	t	Sig.	Model fits	
							RMSE	MAPE
Gold prices	Trend SAR(1)$_{12}$	Constant (η)	10.396	0.773	13.444	<0.001	2.338	11.349
		SAR(1) (ϕ_1)	0.582	0.105	5.523	<0.001		
		Trend (ω)	0.085	0.010	8.490	<0.001		
	Trend SAR(2)$_{12}$	Constant (η)	9.924	0.638	15.548	<0.001	2.298	10.829
		SAR(1) (ϕ_1)	0.822	0.124	6.648	<0.001		
		SAR(2) (ϕ_2)	-0.404	0.107	-3.787	<0.001		
		Trend (ω)	0.087	0.009	10.247	<0.001		
Silver prices	Trend SAR(1)$_{12}$	Constant (η)	17.104	1.022	16.729	<0.001	4.167	16.242
		SAR(1) (ϕ_1)	0.412	0.087	4.728	<0.001		
		Trend (ω)	0.058	0.012	4.840	<0.001		
	Trend SAR(2)$_{12}$	Constant (η)	16.416	0.885	18.546	<0.001	4.140	15.664
		SAR(1) (ϕ_1)	0.488	0.098	4.969	<0.001		
		SAR(2) (ϕ_2)	-0.242	0.091	-2.661	0.009		
		Trend (ω)	0.063	0.011	5.870	<0.001		

TABLE VII
WHITE NOISE TEST OF RESIDUALS FOR COMMODITY GOLD AND SILVER COMMODITY PRICES SERIES

Series	Exponential Mean (α_0)	Kolmogorov-Smirnov Z	Sig.
Gold prices	2.03917	0.596	0.087
Silver prices	3.96541	0.904	0.388

TABLE VIII
COMPARING ARL_1 VALUES ON EXTENDED EWMA AND EWMA CHARTS FOR TREND SAR(2)$_{12}$ MODEL USING GOLD (UNIT: 1,000 USD) AND SILVER (UNIT: USD) COMMODITY PRICES SERIES GIVEN ARL_0 OF 370 AND 500

λ_1	CC	λ_2	UCL	δ								AEQL	PCI
				0.0005	0.001	0.002	0.005	0.01	0.03	0.1	0.5		
Gold prices series with parameters $\alpha_1 = 2.03917(1+\delta), \eta = 9.924, \omega = 0.087, \phi_1 = 0.822, \phi_2 = -0.404$ under ARL_0 OF 370													
0.05	Extended EWMA	0.015	0.01357723	232.23	169.33	109.99	53.90	29.41	10.87	3.90	1.49	0.053	1.351
		0.03	0.00296934	199.60	136.80	84.12	39.30	21.07	7.76	2.88	1.25	0.044	1.116
		0.045	0.00071203	173.72	113.66	67.36	30.58	16.25	6.02	2.32	1.14	0.039	1.000
	EWMA	0	0.0641467	272.65	215.90	152.59	81.50	46.21	17.47	6.16	2.09	0.076	1.927
0.10	Extended EWMA	0.015	0.05904694	251.85	190.99	128.90	65.56	36.34	13.53	4.80	1.72	0.062	1.298
		0.03	0.02711693	232.55	169.66	110.26	54.06	29.50	10.90	3.91	1.49	0.053	1.117
		0.045	0.01254158	215.21	151.84	95.72	45.66	24.66	9.08	3.31	1.35	0.048	1.000
	EWMA	0	0.130267	274.22	217.91	154.62	82.94	47.12	17.83	6.27	2.12	0.077	1.610
0.15	Extended EWMA	0.015	0.1160131	259.71	200.17	137.39	71.09	39.71	14.85	5.24	1.84	0.066	1.242
		0.03	0.0685221	245.71	184.00	122.62	61.58	33.95	12.60	4.48	1.64	0.059	1.101
		0.045	0.0407197	232.82	169.95	110.50	54.20	29.59	10.93	3.92	1.49	0.053	1.000
	EWMA	0	0.1986	275.90	220.02	156.72	84.43	48.07	18.20	6.39	2.14	0.078	1.458
Silver prices series with parameters $\alpha_1 = 3.96541(1+\delta), \eta = 16.416, \omega = 0.063, \phi_1 = 0.488, \phi_2 = -0.242$ under ARL_0 OF 500													
0.05	Extended EWMA	0.015	0.00766377	240.16	158.18	94.18	42.83	22.70	8.28	3.04	1.29	0.045	1.193
		0.03	0.00211138	208.44	131.82	76.15	33.87	17.84	6.54	2.48	1.17	0.041	1.071
		0.045	0.000635135	183.62	112.62	63.69	27.93	14.67	5.42	2.13	1.10	0.038	1.000
	EWMA	0	0.0286126	280.50	195.03	121.35	57.19	30.69	11.19	3.99	1.51	0.054	1.424
0.10	Extended EWMA	0.015	0.02950032	259.38	175.26	106.49	49.21	26.22	9.55	3.45	1.38	0.049	1.149
		0.03	0.01523762	240.27	158.28	94.25	42.87	22.72	8.28	3.04	1.29	0.045	1.063
		0.045	0.0079021	223.34	143.96	84.32	37.88	20.01	7.31	2.72	1.22	0.043	1.000
	EWMA	0	0.0573313	281.08	195.59	121.79	57.43	30.83	11.24	4.00	1.51	0.054	1.270
0.15	Extended EWMA	0.015	0.0552604	266.62	181.93	111.43	51.83	27.68	10.08	3.62	1.42	0.051	1.115
		0.03	0.0354824	252.97	169.46	102.24	46.98	24.99	9.10	3.30	1.35	0.048	1.051
		0.045	0.0228216	240.40	158.39	94.33	42.90	22.74	8.29	3.04	1.29	0.045	1.000
	EWMA	0	0.0862591	281.61	196.13	122.21	57.67	30.96	11.29	4.02	1.52	0.054	1.197

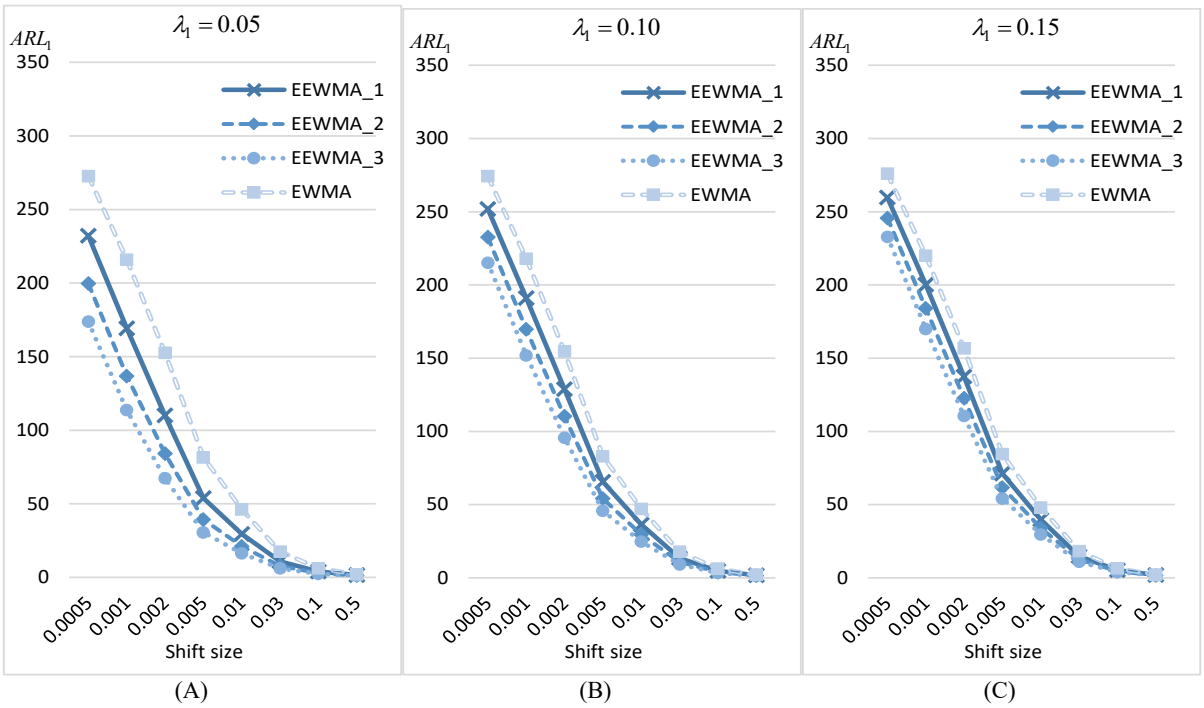

Fig. 1. ARL_1 values on Extended EWMA with different λ_2 and EWMA charts for trend SAR(2)$_{12}$ model when given ; (A) $\lambda_1 = 0.05$, (B) $\lambda_1 = 0.10$, and (C) $\lambda_1 = 0.15$ using Gold prices series from January, 2013 to Apirl, 2025 under $ARL_0 = 370$

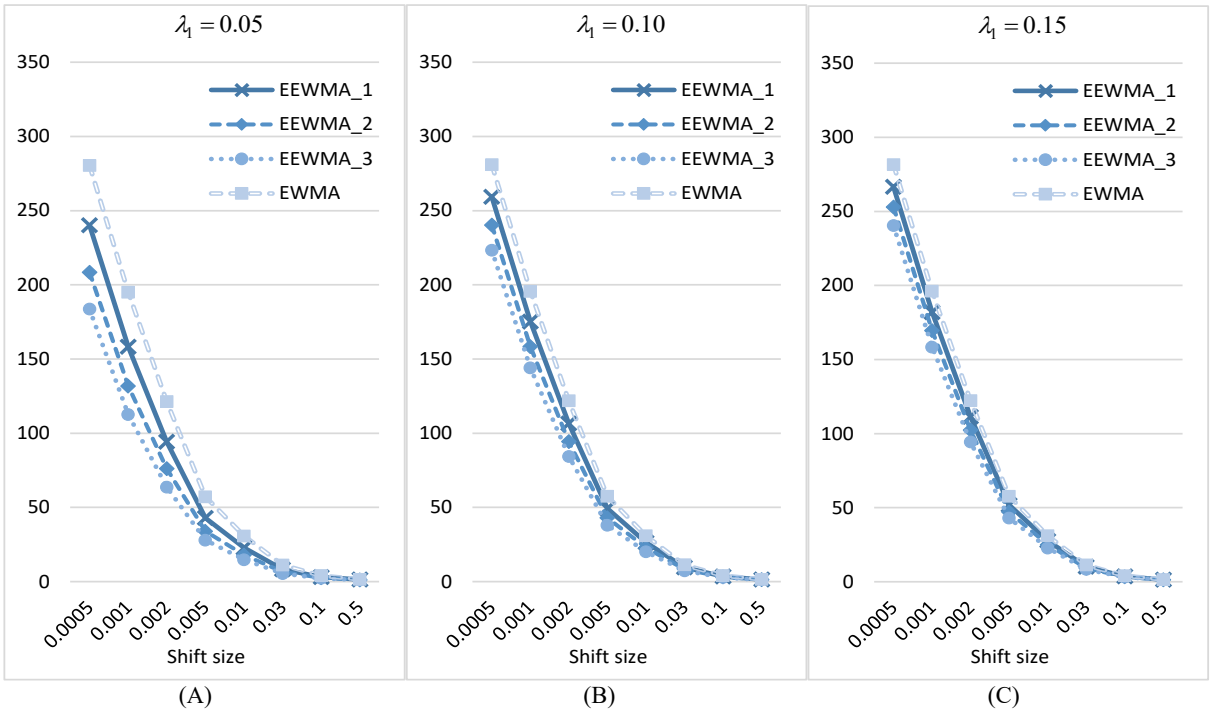

Fig. 2. ARL_1 values on Extended EWMA with different λ_2 and EWMA charts for trend SAR(2)$_{12}$ model when given ; (A) $\lambda_1 = 0.05$, (B) $\lambda_1 = 0.10$, and (C) $\lambda_1 = 0.15$ using Silver prices series from January, 2013 to Apirl, 2025 under $ARL_0 = 500$

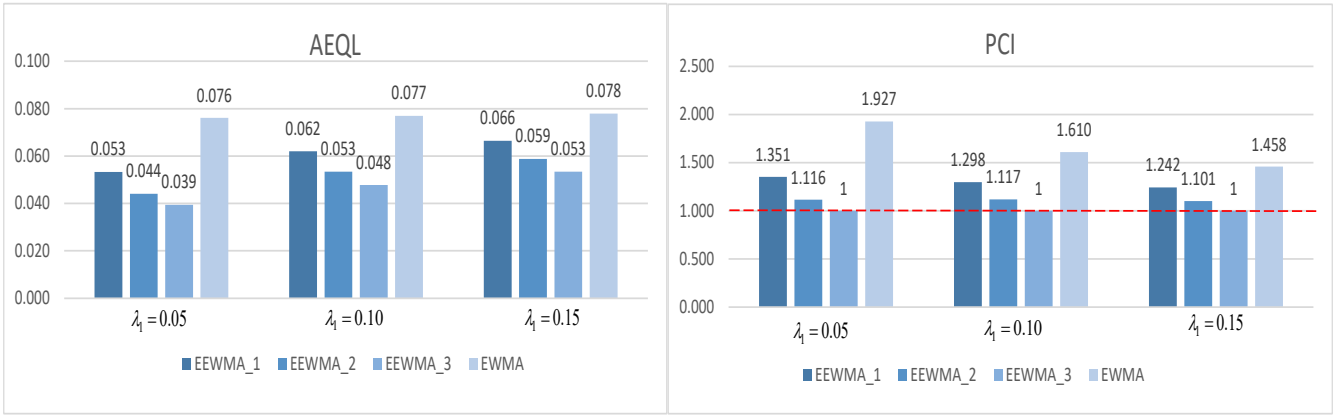

(A)

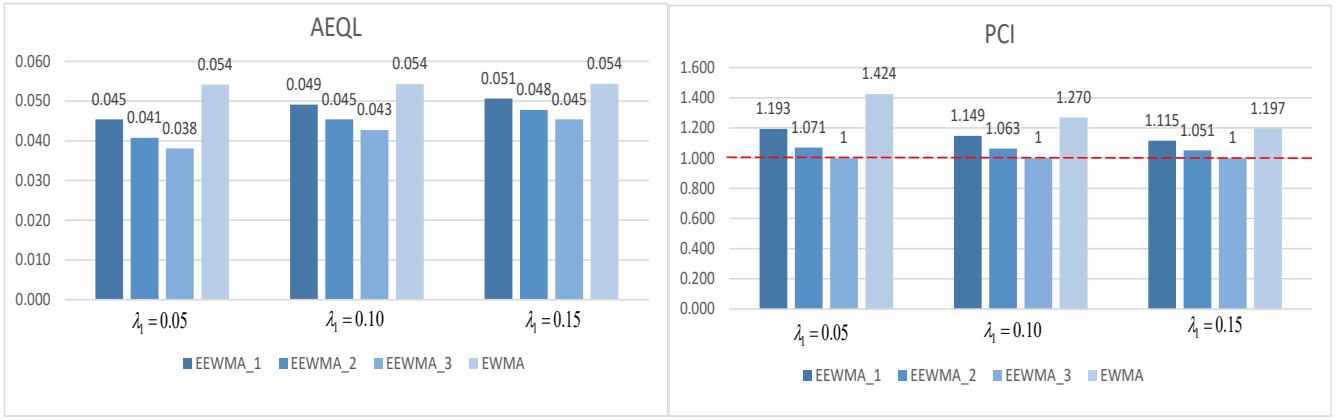

(B)

Fig. 3. AEQL and PCI values on Extended EWMA with different λ and EWMA charts for trend SAR(2)$_{12}$ model by using (A) Gold commodity prices when given ARL_0 of 370 , and (B) Silver commodity prices when given ARL_0 of 500

To be more specific, lower AEQL values show that the chart creates fewer false alarms while retaining a high detection rate. This results in an improvement in the economic efficiency of process monitoring. Additionally, PCI values that are close to or equal to 1 provide further evidence that the process continues to operate well within the constraints of the specification while being controlled by the extended chart. Additionally, a rise in the lower control limit (LCL) results in a minor enhancement of the chart's sensitivity, which is represented in the AEQL and PCI metrics. The chart becomes more responsive to small shifts as the LCL is increased, which enables the detection of subtle process changes to occur more quickly without considerably increasing the number of false alarms encountered.

IV. Applications to Real-World Data

Due to the fact that they serve as dependable stores of value, gold and silver are vital components of the international monetary system. This is especially true during times of economic turbulence. Their market prices are influenced by a wide variety of economic and geopolitical events, including variations in interest rates, currency movements, and trends in inflation. In order to protect themselves from potential financial losses, investors and institutions frequently make use of these metals as hedging strategies.

A consequence of this is that fluctuations in their pricing have the potential to impact decisions about monetary policy, investment behavior, and the overall stability of the economy. The result of this is that price series of gold and silver are utilized as input data for the purpose of monitoring variations through the utilization of control chart approaches.

Two commodity price series were the primary focus of the investigation. These were gold (measured in units of one thousand US dollars) and silver (measured in US dollars).

A real data analysis was conducted using monthly observations fitted to trend SAR(P)$_L$ models. Two case studies were examined, both employing the extended EWMA control chart and comparing its performance to that of the traditional EWMA control chart.

The dataset consists of 148 monthly observations of gold and silver prices, covering the period from January 2013 to April 2025. These time series were retrieved from the website https://th.investing.com/commodities.

Table VIII presents the findings from the analysis of the real data. Fitting the trend SAR model was accomplished with the help of SPSS, and the calculated coefficients of the model are shown in Table VI. The model that gave the lowest values for both of these criteria was selected as the winner. The Root Mean Squared Error (RMSE) and the Mean Absolute Percentage Error (MAPE) were the two metrics that were utilized in the selection process. To

determine whether the residuals follow an exponential distribution, researchers evaluated and applied the Kolmogorov–Smirnov (K–S) test. The goodness-of-fit test yielded the following findings, as presented in Table VII.

As a result of the aforementioned test, the model was derived as follows:

Dataset I : Gold Prices series
It was determined as trend SAR(2)$_{12}$ model, its equation is expressed as follows:

$$Y_t = 9.924 + 0.087t + 0.822Y_{t-12} - 0.404Y_{t-24} + \xi_t$$

where $\xi_t \sim Exp(2.03917)$

Dataset II : Silver Prices series
It was determined as trend SAR(2)$_{12}$ model, its equation is expressed as follows:

$$Y_t = 16.416 + 0.063t + 0.488Y_{t-12} - 0.242Y_{t-24} + \xi_t$$

where $\xi_t \sim Exp(3.96541)$

Table VIII presents the ARL_1 results from fitting the trend SAR(2)$_{12}$ model to the gold price series (with an initial ARL_0 set at 370) and the silver price series (with an initial ARL_0 set at 500). The analysis of lower and upper control limits was performed over the interval [0.0001,UCL], with s and s' representing the upper limits for the extended EWMA and conventional EWMA charts, respectively. The findings demonstrate that the extended EWMA control chart with a fixed value of $\lambda_1 = 0.05$ consistently outperformed the alternatives. When evaluated individually by λ_1, the extended EWMA chart with the optimal fixed $\lambda_2 = 0.045$ yielded the lowest ARL_1, outperforming both other extended EWMA configurations and the conventional EWMA chart. Furthermore, a reduction in λ_2, particularly as it approaches zero, was associated with a decrease in ARL_1. In light of this, it appears that the responsiveness in detecting shifts in the process mean has been improved. Across all of the scenarios that were investigated, these tendencies were consistently seen. An illustration of the ARL1 values that match the different shift magnitudes can be found in Figures 1 and 2. This set of graphs provides a visual representation of the performance of various configurations of the extended EWMA control chart under a variety of different circumstances.

The findings demonstrate that the extended EWMA chart with a fixed value of $\lambda_1 = 0.05$ consistently outperformed other alternatives. When evaluated individually by λ_1, the configuration with the optimal fixed value of $\lambda_2 = 0.045$ and $\lambda_1 = 0.05$ resulted in distinctly lower ARL_1 values across all shift magnitudes, indicating faster detection of process changes. In contrast, when using $\lambda_1 = 0.10$ or $\lambda_1 = 0.15$, the ARL_1 values across various scenarios tended to converge and showed minimal variation, implying lower sensitivity. This was particularly evident for $\lambda_1 = 0.15$, where the ARL_1 curves were closely clustered, regardless of shift size. In summary, the configuration with $\lambda_1 = 0.05$ demonstrated superior detection performance and sensitivity, making it a more effective choice for monitoring small to moderate process shifts.

It is important to note that EEWMA_1, EEWMA_2, and EEWMA_3 correspond to λ_2 values of 0.015, 0.03, and 0.045, respectively. Upon examining the AEQL and PCI values, the results demonstrate the effectiveness of the extended EWMA chart (with fixed $\lambda_1 = 0.05$ and $\lambda_2 = 0.045$) as it consistently yields the lowest AEQL values and a PCI score of 1 for every λ_1 based on both two dataset. The effectiveness of the control chart is supported by the AEQL and PCI values, as shown in Fig.3. Besides, the results were also consistent with those obtained from the simulated data. This finding is consistent with the results of Karoon et al. [29], who previously investigated control charts under a SAR(P)$_L$ model without incorporating the trend component

Accordingly, Fig. 4 illustrates the performance of the control charts in detecting process shifts during monitoring, based on the dataset I: the gold prices series, by plotting the control chart graphs. The results show that the extended EWMA control chart (with fixed $\lambda_1 = 0.05$ and $\lambda_2 = 0.045$), developed using the trend SAR(2)$_{12}$ model and with an initial in-control ARL set at 370, signaled the first out-of-control condition at the 92nd observation. In contrast, the traditional EWMA control chart (with fixed $\lambda_1 = 0.05$ and $\lambda_2 = 0$) signaled the first out-of-control condition at the 140th observation. These results are illustrated in Fig. 4 (A). Similarly, for Dataset II: the silver price series, the control chart graphs were plotted to evaluate monitoring performance. The extended EWMA control chart (with fixed $\lambda_1 = 0.05$ and $\lambda_2 = 0.045$), developed using the same trend SAR(2)$_{12}$ model as previously described but initialized with an in-control ARL of 500, detected the first out-of-control signal at the 1st observation. In contrast, the traditional EWMA chart (with fixed $\lambda_1 = 0.05$ and $\lambda_2 = 0$) detected the shift later, at the 143rd observation. These results are illustrated in Fig. 4 (B). The results of this study highlight the superior responsiveness of the extended EWMA control chart in detecting small process shifts more promptly than the traditional EWMA chart, particularly in datasets exhibiting autocorrelation.

V. Conclusion

The performance of the control charts was assessed using the Average Run Length (*ARL*). The explicit formulas serve as an effective alternative for evaluating the *ARL* in trend SAR(P)$_L$ processes applied to extended EWMA control charts. Although the *ARL* values obtained from the explicit formulas closely match those derived from the Numerical Integral Equation (NIE) method, with Absolute Percentage Relative Error (APRE) values approaching zero, the explicit formulas provide a significant advantage in terms of reduced computational time. For small shift sizes, the *ARL* obtained from the explicit formulas on the extended EWMA control chart with fixed $\lambda_1 = 0.05$ demonstrates a high level of sensitivity, enabling earlier detection of process changes compared to other configurations.

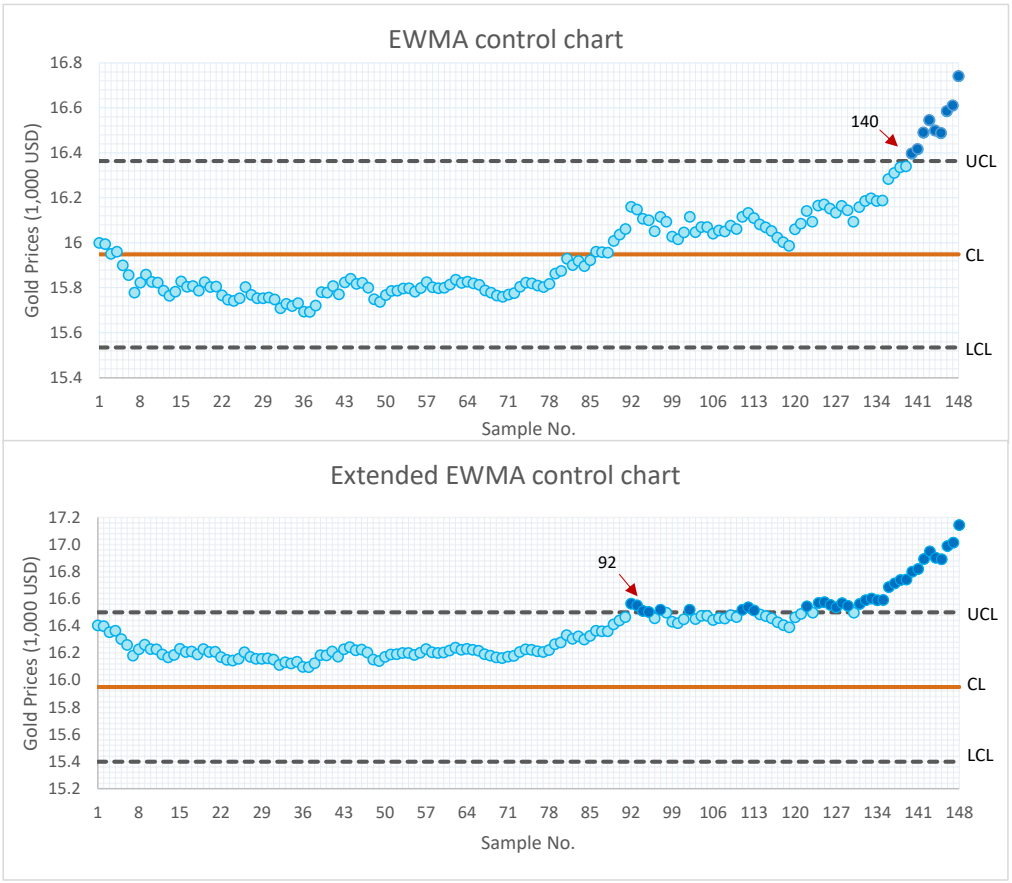

(A)

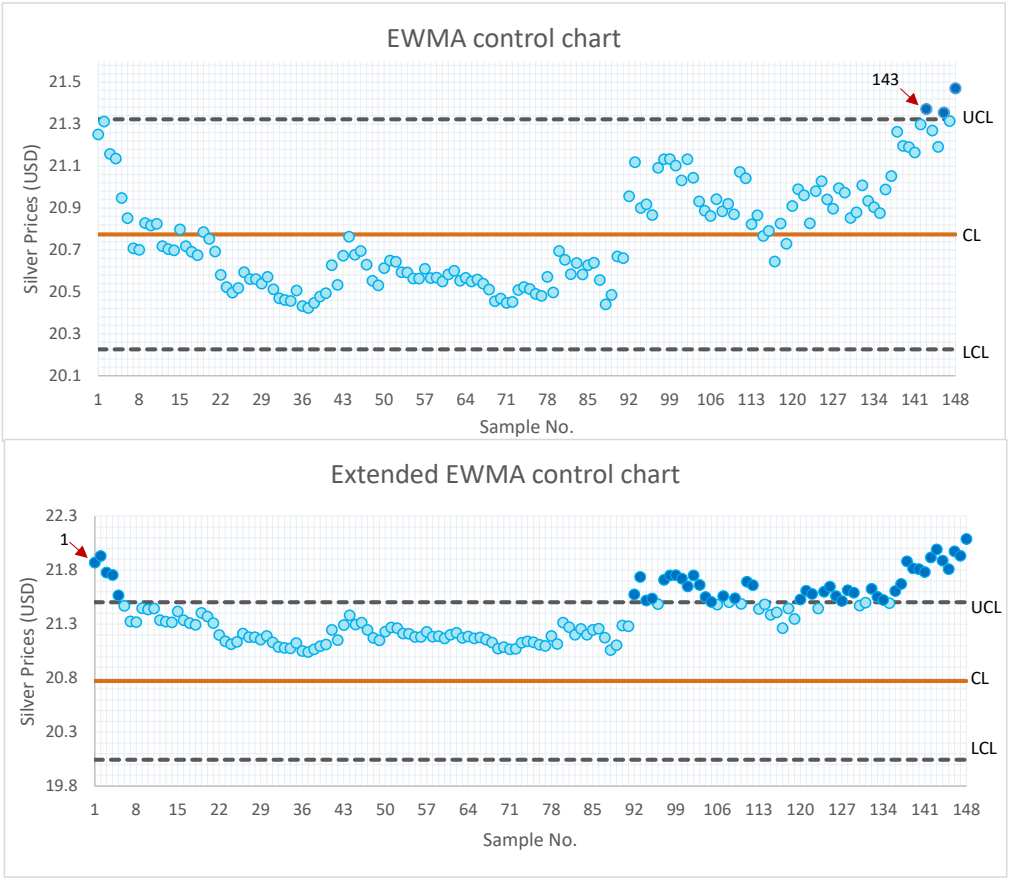

(B)

Fig. 4. Performance of Extended EWMA () and EWMA charts for detecting changes based on trend SAR(2)$_{12}$ model by using (A) Gold prices series , and (B) Silver prices series, covering the Period from January 2013 to April 2025

Moreover, A decrease in ARL_1 correlated with a decrease in λ_2 , especially as it gets closer to zero, suggesting increased responsiveness in identifying changes in the process mean. These patterns were consistently observed across all scenarios examined under the trend $SAR(P)_L$ model. In addition, AEQL and PCI were utilized to check the effectiveness of ARL when it was running on the extended EWMA chart (with fixed $\lambda_1 = 0.05$). A decrease in λ_2, particularly as it approaches zero, was found to further enhance detection capability. When compared to the traditional EWMA chart, the extended EWMA control chart persistently exhibits higher sensitivity in identifying process shifts. All the tested scenarios, including shifts of varying degrees of magnitude, demonstrate this. The capacity of this system to assign greater weight to new observations while keeping memories of previous data is the reason for its improved performance. This feature makes it particularly useful in contexts that are dynamic or trending. When applied to data from the actual world that follows a pattern, the findings also suggest that the explicit formula method is effective. The results that are produced by the Seasonal Autoregressive model of order P and seasonal lag L ($SAR(P)_L$) are extremely similar to the results that are created by simulated datasets. This consistency highlights the resilience and practical application of the analytical technique that has been provided, particularly in real-world situations such as economics, energy, and environmental monitoring, where seasonal trends and autocorrelation are present with respect to the data.

Using real-world time series data for gold and silver prices, this study further evaluated the efficiency of control charts in detecting shifts in process means. The data was collected from the market. According to the findings of the analysis, the expanded EWMA control chart, in particular when it is implemented with the explicit analytical formula, displays a considerable improvement in both the sensitivity and speed of detecting tiny mean shifts in comparison to the regular EWMA control chart. There are several applications that involve financial and economic indicators, such as commodity market surveillance, investment risk monitoring, and economic trend forecasting, where the early identification of minor changes can be vital. This improvement is especially relevant in these applications.

The empirical findings have demonstrated the practical applications of the suggested method in the field of financial time series analysis. This underscores the method's potential for broader application in fields typified by non-stationary, seasonal, and autocorrelated data structures. The approach could be extended to include more financial variables such as crude oil prices, exchange rates, and inflation indices in the future research directions. This would allow for an evaluation of the generalizability, scalability, and robustness of the model regardless of the market conditions that are present. Even further, the incorporation of adaptive control charts or other time-series-based modeling techniques has the potential to significantly improve the real-time responsiveness and dependability of change detection mechanisms, particularly in situations that are volatile and dynamic.

Nevertheless, researchers examined the efficiency of control charts in identifying shifts in process methods by utilizing actual data from gold and silver price series. When compared to the conventional EWMA chart, the results demonstrate that the extended EWMA control chart, particularly when strengthened by the explicit formula approach, provides a higher level of sensitivity and a more rapid discovery of even minute shifts. This research is especially useful for monitoring financial and economic indicators in situations when early identification is essential, such as in the trading of commodities, the evaluation of investment risk, and the forecasting of economic conditions. For the purpose of determining the generalizability and robustness of the strategy, it is possible that future research will extend this approach by applying it to other financial time series. These time series could include crude oil prices, currency rates, and inflation indices. Utilizing adaptive control charts or another time series-based model may further enhance the capability to identify changes in real time within dynamic and unpredictable environments.

APPENDIX

This study applies Banach's Fixed Point Theorem [33] to demonstrate the existence and uniqueness of the *ARL* solution for the extended EWMA control chart under the trend $SAR(P)_L$ process. The procedure is outlined as follows. Define the operator T on the space of continuous functions such that its fixed point corresponds to the desired *ARL* solution, as presented in Eq. (13) below.

$$T\left(\vartheta(\varpi)\right) = 1 + \frac{1}{\lambda_1}\int_r^s \vartheta(\psi) f\left(\frac{\psi - \mathrm{A}\varpi + \lambda_2 Y_{1-1L}}{\lambda_1} - \theta\right) d\psi. \quad (13)$$

If the operator T is a contraction mapping, then the fixed-point equation $T\left(\vartheta(\varpi)\right) = \vartheta(\varpi)$ admits a unique solution. The theorem can be applied as follows to demonstrate the existence of Eq. (13) and its unique solution [34,25].

Theorem 1 Banach's Fixed-point Theorem: Let Y be a complete metric space and $T: Y \to Y$ be a contraction mapping with contraction constant $k \in [0,1)$ such that $\left\|T\left(\vartheta(\varpi)_1\right) - T\left(\vartheta(\varpi)_2\right)\right\| \le k\left\|\vartheta(\varpi)_1 - \vartheta(\varpi)_2\right\|$, $\forall\, \vartheta(\varpi)_1, \vartheta(\varpi)_2 \in Y$. Then there exists a unique $\vartheta(\cdot) \in Y$ such that $T\left(\vartheta(\varpi)\right) = \vartheta(\varpi)$, i.e., a unique fixed-point in Y .

Proof: Let T defined in (13) is a contraction mapping for $\vartheta(\varpi)_1, \vartheta(\varpi)_2 \in \varpi[r,s]$.

$$\left\|T(\vartheta(\varpi)_1) - T(\vartheta(\varpi)_2)\right\|_\infty = \sup_{\varpi\in[r,s]} \left|\vartheta(\varpi)_1 - \vartheta(\varpi)_2\right|$$

$$= \sup_{\varpi\in[r,s]} \left|\frac{\mathrm{H}(\varpi)}{\lambda_1\alpha}\right| \int_r^s \left(\left(\vartheta(\psi)_1 - \vartheta(\psi)_2\right)\cdot \Lambda_0(\psi)\right) d\psi$$

$$= \sup_{\varpi\in[r,s]} \left|\frac{\mathrm{H}(\varpi)}{\lambda_1\alpha}\right| \int_r^s \left(\left(\vartheta(\psi)_1 - \vartheta(\psi)_2\right)\cdot \Lambda_0(\psi)\right) d\psi$$

$$\le \sup_{\varpi\in[r,s]} \left\|T(\vartheta(\psi)_1) - T(\vartheta(\psi)_2)\right\|_\infty \mathrm{H}(\varpi)\left(\Lambda_0(s) - \Lambda_0(r)\right)$$

$$= \left\| T(\vartheta(\psi)_1) - T(\vartheta(\psi)_2) \right\|_\infty \sup_{\varpi \in [r,s]} \left| \mathrm{H}(\varpi) \right| \left| \Lambda_0(s) - \Lambda_0(r) \right|$$

$$\leq k \left\| T(\vartheta(\psi)_1) - T(\vartheta(\psi)_2) \right\|_\infty$$

where $k = \sup_{\varpi \in [r,s]} \left| \mathrm{H}(\varpi) \right| \left| \Lambda_0(s) - \Lambda_0(r) \right|; k \in [0,1)$.

REFERENCES

[1] W.A. Shewhart. Quality control charts, Bell System Technical Journal, Vol. 5, No. 4, 593-603, 1926.

[2] E.S. Page. Continuous inspection schemes, Biometrika, Vol. 41, No. 1-2, 100-115, 1954.

[3] W.S. Roberts. Control chart tests based on geometric moving averages, Technometrics, Vol. 1, No. 3, 239-250, 1959.

[4] N. Khan, M. Aslam, C.H. Jun. Design of a control chart using a modified EWMA statistic, Quality and Reliability Engineering International, Vol. 33, No. 5, 1095-1104, 2017.

[5] A.K. Patel, J. Divecha. Modified exponentially weighted moving average (EWMA) control chart for an analytical process data, Journal of Chemical Engineering and Materials Science, Vol. 2, 12-20, 2011.

[6] A.A. Mahmoud, W.H. Woodall. An evaluation of the double exponentially weighted moving average control chart, Communications in Statistics-Simulation and Computation, Vol. 39, No. 5, 933-949, 2010.

[7] S.E. Shamma, A.K. Shamma. Development and evaluation of control charts using double exponentially weighted moving averages, International Journal of Quality Reliability Management, Vol. 9, No. 6, 18-25, 1992.

[8] M. Naveed, M. Azam, N. Khan, M. Aslam. Design of a control chart using extended EWMA statistic, Technologies, Vol. 4, No. 6, 108-122, 2018.

[9] M. Waqas, S. H. Xu, S. Hussain, and M. U. Aslam. Control charts in healthcare quality monitoring: A systematic review and bibliometric analysis, International Journal for Quality in Health Care, Vol. 36, No. 3, Article mzae060, 2024.

[10] S. M. M. Raza, M. H. Sial, N. U. Hassan, G. T. Mekiso, Y. A. Tashkandy, and M. E. Bakr. Use of improved memory type control charts for monitoring cancer patients' recovery time censored data, Scientific Reports, Vol. 14, Article 5604, 2024.

[11] K. Bisiotis, S. Psarakis, and A. N. Yannacopoulos. Control charts in financial applications: An overview, Quality and Reliability Engineering International, Vol. 38, No. 1, 175, 2021.

[12] J. Lim and S. Lee. Efficient ARL estimation for general control charts using censored run lengths, Quality Engineering, 2024.

[13] J. C. Fu, F. A. Spiring, and H. Xie. On the average run lengths of quality control schemes using a Markov chain approach, Statistics & Probability Letters, Vol. 56, No. 4, 369–380, 2002.

[14] K. Karoon, Y. Areepong, S. Sukparungsee. Numerical integral equation methods of average run length on extended EWMA control chart for autoregressive process. In proceesing of International Conference on Applied and Engineering Mathematics, London, England, 51-56, 2021.

[15] K. Petcharat. Designing the performance of EWMA control chart for seasonal moving average process with exogenous variables, IAENG International Journal of Applied Mathematics, Vol. 53, No. 2, 757–765, 2023.

[16] C. Chananet and S. Phanyaem. Improving CUSUM control chart for monitoring a change in processes based on seasonal ARX model, IAENG International Journal of Applied Mathematics, Vol. 52, No. 3, 589–596, 2022.

[17] J. Chen. Time Series Analysis and Forecast of Sales of New Car and Used Car Using SARIMA Model, Advances in Economics Management and Political Sciences, Vol. 86, No. 1, 122–132, 2024.

[18] K. K. Rono, D. K. Muriithi, and D. M. Mwangi. Forecasting the incidence of dengue fever in Malaysia: A comparative analysis of seasonal ARIMA, dynamic harmonic regression, and neural network models, International Journal of Advanced and Applied Sciences, Vol. 11, No. 1, 20–31, 2024.

[19] W. Suriyakat and K. Petcharat. Exact Run Length Computation on EWMA Control Chart for Stationary Moving Average Process with Exogenous Variables, Mathematics and Statistics, Vol. 10, No. 3, 624–635, 2022.

[20] L. Zhang, S. Suraphee, and P. Busababodhin. Derivation of Explicit Formulae for Performance Measures of CUSUM Control Chart for SMA(Q)s Model with Exponential White Noise, Lobachevskii Journal of Mathematics, Vol. 44, No. 9, 3902–3913, 2023.

[21] K. Raweesawat and S. Sukparungsee. Explicit Formulas of ARL on Double Moving Average Control Chart for Monitoring Process Mean of ZIPINAR(1) Model with an Excessive Number of Zeros, International Journal of Science and Technology, Vol. 17, No. 1, 1–15, 2024.

[22] W. Peerajit. Determining the ARL for a Shift in the Mean of a Long-Memory ARFIMA(1, d, 1)(1, D, 1)s Process with Exponential White Noise Running on a CUSUM Control Chart, Thailand Statistician, Vol. 22, No. 2, 407–429, 2024.

[23] S. Phanyaem. Precise Average Run Length of an Exponentially Weighted Moving Average Control Chart for Time Series Model, Thailand Statistician, Vol. 22, No. 4, 909–925, 2024.

[24] T. Muangngam, Y. Areepong, and S. Sukparungsee. Performance Evaluation of Extended EWMA Chart for AR Model with Exogenous Variables, HighTech and Innovation Journal, Vol. 5, No. 4, 899–910, 2024.

[25] R. Sunthornwat, Y. Areepong, and S. Sukparungsee. Analytical Explicit Formulas of Average Run Length of DEWMA Control Chart based on Seasonal Moving Average Process, WSEAS Transactions on Systems, Vol. 24, 1–15, 2025.

[26] K. Karoon and Y. Areepong. The efficiency of the new extended EWMA control chart for detecting changes under an autoregressive model and its application, Symmetry, Vol. 17, No. 1, Article 104, 2025.

[27] K. Petcharat. The Effectiveness of CUSUM Control Chart for Trend Stationary Seasonal Autocorrelated Data, Thailand Statistician, Vol. 20, No. 2, pp. 475–488, 2022.

[28] K. Karoon, Y. Areepong, and S. Sukparungsee. Exact Run Length Evaluation on Extended EWMA Control Chart for Seasonal Autoregressive Process, Engineering Letters, Vol. 30, No. 4, 1377–1390, 2022.

[29] Y. Areepong and K. Karoon. Detection Capability of the DEWMA Chart Using Explicit Run Length Solutions: A Case Study on Data of Gross Domestic Product, Engineering Letters, Vol. 32, No. 7, 1300–1312, 2024.

[30] S. Sukparungsee and Y. Areepong. The Exact Solution of ARL using an Integral Equation on the DMEWMA Chart for the SAR(P)L Process for Mean Shift Detection, WSEAS Transactions on Systems, Vol. 24, 1–15, 2025.

[31] K. Karoon, Y. Areepong, and S. Sukparungsee. Exact Run Length Evaluation on Extended EWMA Control Chart for Seasonal Autoregressive Process, Engineering Letters, Vol. 30, No. 4, 1377–1390, 2022.

[32] M. Almousa. Adomian decomposition method with modified Bernstein polynomials for solving nonlinear Fredholm and Volterra integral equations, Mathematics and Statistics, Vol. 18, No. 3, 278–285, 2020.

[33] S. Shukla, S. Balasubramanian, and M.A. Pavlovic. Generalized Banach fixed point theorem, Bulletin of the Malaysian Mathematical Sciences Society, Vol. 39, 1529–1539, 2016.

[34] Y. Areepong, and K. Karoon. Developed ARL by integral equation solutions to monitor changes under autocorrelated data for the DEWMA chart, IAENG International Journal of Applied Mathematics, Vol. 54, No. 8, 1631–1642, 2024.

[35] K. Petcharat. Designing the performance of EWMA control chart for seasonal moving average process with exogenous variables, IAENG International Journal of Applied Mathematics, Vol. 53, No. 2, 757–765, 2023.